

Dynamics of the Salton block: Absolute fault strength and crust-mantle coupling in Southern California

Noah Fay
Eugene Humphreys } Department of Geological Sciences, University of Oregon, Eugene, Oregon 97403, USA

ABSTRACT

Analysis of force and torque balance on the Salton block, Southern California, yields estimates of time-averaged shear stress acting on the bounding faults and the base of the crust. Averaged over a depth of 30 km, the San Andreas and San Jacinto faults sustain time-averaged shear stress of ~21–35 and 24–43 MPa, respectively. This implies that tectonic shear stress at seismogenic depths is greater than a typical 1–10 MPa earthquake stress drop and, with a corresponding effective friction coefficient of 0.10–0.21, lower than that predicted by laboratory experiments. Basal stress of 3–14 MPa also is required to drive the Salton block into the Transverse Ranges. Thus, the forces driving mountain building, basin formation, and the generation of earthquakes south of the Transverse Ranges in Southern California stem from stresses transmitted laterally across weak faults and from below.

Keywords: crustal deformation, crust-mantle coupling, fault strength, stress.

INTRODUCTION

The Salton block, Southern California (Fig. 1), is bound by the right-lateral San Jacinto fault and San Andreas fault. Forces acting on this block are transmitted across faults as a result of tectonic loading and gravitational potential energy variations caused by topography and heterogeneous lithospheric density structure. Additional forces are applied at the base of the block as a result of relative crust-mantle motion. When balancing the forces and torques acting on this block, the presence of significant and quantifiable gravitational potential energy variations associated with the Transverse Ranges topography provides absolute stress estimates that allow us to assess two outstanding questions of crustal deformation and lithospheric dynamics in Southern California.

First, although the coseismic stress drop is known to be 1–10 MPa (Kanamori and Anderson, 1975), the absolute, time-averaged tectonic stress level (fault strength) on faults such as the San Andreas fault is debated. This strength is important to our understanding of fault physics and how stresses are transmitted across plate boundaries (e.g., Lachenbruch and Sass, 1992). In situ borehole stress measurements (Townend and Zoback, 2000) consistent with laboratory derived friction coefficients of ~0.6–1.0 (Byerlee, 1978) suggest that the crust in general is strong and supports stresses of ~100 MPa. Scholz (2000), on the basis of the rotation of stress axes in Southern California (Hardebeck and Hauksson, 1999), suggested that the San Andreas fault is similarly as strong as the ambient crust, although Townend and Zoback (2001) questioned this conclusion. Furthermore, the partial entrain-

ment of the Sierra Nevada block with the Pacific plate and NW-oriented extension of the Basin and Range (Atwater, 1970; Thatcher et al., 1999) also suggest that the mature San Andreas fault margin is sufficiently strong to transmit the stresses required for this tectonic activity.

The lack of a frictionally generated heat-flow anomaly near the San Andreas fault (Lachenbruch and Sass, 1980, 1992; Saffer et al., 2003) and the common occurrence of maximum horizontal compressive stresses oriented at high angles to the San Andreas fault (Mount and Suppe, 1987; Zoback et al., 1987; Townend and Zoback, 2001, 2004), however, suggest that the San Andreas fault is frictionally weak and slips under relatively low depth-averaged shear stress of $\leq \sim 20$ MPa.

Second, to what degree is upper crustal deformation driven by stresses transmitted laterally across faults, and to what degree from below by basal stresses (e.g., Jackson, 2002)? Ideal transform tectonics would be driven by stresses transmitted from the far field and exhibit no net change in area. However, significant thrust faulting and mountain building in Southern California suggest that this is not such an ideal transform environment. Although the “Big Bend” geometry of the San Andreas system kinematically accounts for the thrust faulting and mountain building, it does not explain why the lithosphere maintains this apparently energetically unfavorable plate-margin geometry (Kosloff, 1977). The Cerro Prieto–Laguna Salada–Elsinore fault system (Fig. 1) is more favorably aligned and would allow for Pacific–North America motion while avoiding much of the energy expense of mountain building, yet the Elsinore fault is

only a minor component of the Southern California fault system; the majority of dextral slip is accommodated by the more easterly San Jacinto and San Andreas faults (Bennett et al., 2004; Fay and Humphreys, 2005). Convergence and downwelling of the lithospheric mantle beneath the greater Transverse Ranges crust may apply basal tractions that drive crustal blocks toward the Transverse Ranges (Bird and Rosenstock, 1984; Humphreys and Hager, 1990; Houseman et al., 2000).

FORCE AND TORQUE BALANCE

Loads driving fault-parallel northwest motion of the Salton block, shown with black arrows in Figure 1 (see Table 1), include shear stress transmitted across the San Jacinto fault and fault-parallel basal tractions related to relative crust-mantle motion. Resisting loads include San Andreas fault shear stress, frictional resistance of thrust faulting at the leading edge of the block, extensional faulting at the trailing edge in the Brawley seismic zone, the ex-

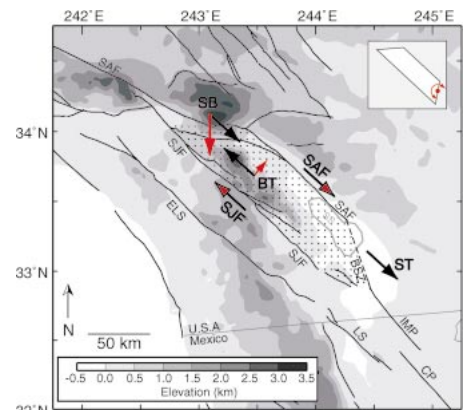


Figure 1. Map of study area showing topography, major faults (solid lines), and loads that force (black arrows) and torque (red arrows) the Salton block (stippled). Compressional and/or extensional faulting in Banning and Brawley seismic zones (BSZ) (arrows not shown for clarity) provide resisting forces parallel to San Andreas fault (SAF). Simplified geometry used in calculations is shown to scale in inset and torque is calculated about red dot. SJF—San Jacinto fault; ELS—Elsinore fault; LS—Laguna Salada fault; IMP—Imperial fault; CP—Cerro Prieto fault; SB—San Bernardino Mountains; ST—Salton Trough basin; BT—basal tractions; SS—Salton Sea. Figure created with Generic Mapping Tools of Wessel and Smith (1998).

TABLE 1. LOADS ACTING ON THE SALTON BLOCK SEPARATED INTO THOSE THAT DRIVE/RESIST NW BLOCK MOTION AND TORQUE THE BLOCK

	Driving Force	Resisting Force
Clockwise Torque	San Jacinto fault strength	San Andreas fault strength
Counterclockwise Torque	Basal Traction	
No Torque		San Bernardino Mtn. PE Salton Trough sedimentary basin PE Banning thrust faults Brawley Seismic Zone

cess potential energy of the San Bernardino Mountains, and low potential energy of the sediment-filled Salton Trough. These loads also torque the block, as shown with red arrows in Figure 1. The dextral San Andreas fault and San Jacinto fault both produce clockwise torque, as do fault-perpendicular basal tractions resulting from counterclockwise rotation of the crust relative to underlying mantle. This latter traction is a result of the mantle converging on the axis of the Transverse Ranges (where it sinks), whereas the crust avoids much of the convergence by tending to follow the San Andreas fault around the Big Bend (Humphreys and Hager, 1990). These clockwise torques are balanced largely by counterclockwise torque caused by the oblique convergence of the Salton block into the Transverse Ranges Mountains. For this effectively instantaneous model, we ignore the tectonic effects of erosion and isostatic adjustment (e.g., Willett and Brandon, 2002).

We calculate the force and torque created by each load according to the following geological constraints and simplifying assumptions. In all cases we assume that the block is 30 km thick, the approximate Moho depth in this region (Zhu and Kanamori, 2000). The crustal root imaged beneath the San Bernardino Mountains (Zhu and Kanamori, 2000) implies that the mountains are in near Airy isostasy and thus ~30 km also represents the depth over which uniform pressure caused by the excess mass of the mountains acts (e.g., Molnar and Lyon-Caen, 1988). Fault loads are calculated as a depth-average shear stress times fault area. The San Jacinto fault and San Andreas fault are 160 and 100 km long, respectively. Assuming optimally oriented faults under hydrostatic pore pressure with a friction coefficient of ~0.2 (determined in our analysis to be self-consistent with the results), the thrust fault in the Banning region (immediately south of the San Bernardino Mountains) and normal faults in the Brawley seismic zone (Fig. 1) are constrained to be 1.3 and 0.75, respectively, times as strong as the similarly organized San Jacinto fault (e.g., Lachenbruch and Sass, 1992). These loads are included in force balance calculations but ignored in torque balance calculations because they are largely parallel to the San Andreas fault and produce insignificant torque. We calculate

torque about the SE end of the Salton block (red dot in Fig. 1 inset) as this is the approximate pivot point of rotation of the upper crust relative to the underlying mantle (Humphreys and Hager, 1990, their Fig. 4). Clockwise torque caused by NE-directed, fault-perpendicular, basal stress is thus modeled as maximum at the NW end of the block and linearly tapers to zero at the SE end.

The topographic loads are calculated as $\Delta\rho gh \times \text{area}$ of the block face adjacent to the mountains (or antimountains for the Salton Trough basin), where $\Delta\rho$ is the density anomaly, g is acceleration due to gravity, and h is the height. We use $\Delta\rho = 2750 \text{ kg/m}^3$ and $h = 1.5 \text{ km}$ for the San Bernardino Mountains. Thrust faults beneath the mountains having dip angle δ provide a mechanical advantage of $\tan(\delta)$ for elevating mass so that the force necessary to lift the mountains is proportional to $\Delta\rho gh \tan(\delta)$. We use $\delta = 45^\circ$ based on the approximate dip angle of the Banning fault (Jones et al., 1986), and assume that faulting extends to 15 km and that below 15 km shortening is accommodated viscously by pure shear. Then the force required to lift the topographic load is $\Delta\rho g(h/2) \times \text{area} \times [1 + \tan(45^\circ)]$. Note that by choosing $\delta = 45^\circ$, the inclusion of the mechanical advantage $\tan(\delta)$ term is inconsequential.

The Salton Trough sedimentary basin at the trailing edge of the Salton block is composed of ~5 km of low-density sediments underlain by ~5–7 km of metasediments. These basin rocks are less dense than the surrounding crustal rocks by ~100–450 kg/m^3 (Fuis et al., 1982; Lachenbruch et al., 1985). We approximate the basin with $\Delta\rho = 250 \text{ kg/m}^3$ uniformly over $h = 10 \text{ km}$.

The results of summing force and torque are given in Figure 2. With the possible exception of the point about which we have calculated torque, reasonable variations in model inputs such as crustal density and basin depth have small effects on the results shown in this plot. Because the problem is underdetermined (we have two equations [zero sum of force and torque] and effectively four unknowns [San Jacinto and San Andreas fault strength and two components of basal traction]), we show the results as the range of fault strength and basal traction values that satisfy force and torque balance. Force balance in the fault-

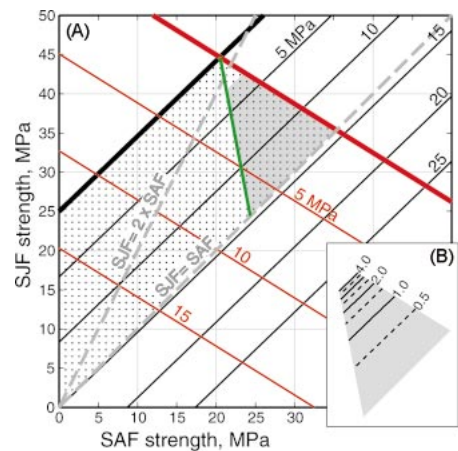


Figure 2. A: Force and torque balance shown as functions of strength of San Andreas fault (SAF) and San Jacinto fault (SJF). Black stress labels indicate magnitude of uniform basal tractions acting in fault-parallel direction (Fig. 1). Red labels indicate maximum fault-perpendicular tractions at NW end of block that taper linearly to zero at SE end. Zero sums of forces and torques, and constraints from crust-mantle kinematics, limit acceptable range of fault strengths (averaged over 30 km) and basal tractions to within shaded region. This region limits ratio of San Jacinto fault to San Andreas fault strengths from 1 to maximum of ~2 (dashed gray lines). B: Relative importance of fault and basal tractions. Shaded region is from A. Lines show contours (increments of 0.5) of ratio of net driving force (driving minus resisting) applied to block from frictional faults to driving force applied by basal tractions. Zero contour is just outside shaded region (lower right). Large value indicates that basal forces are negligible compared to forces transmitted laterally by faults. Small values (<1) indicate that basal forces are most important. Figure created with Generic Mapping Tools of Wessel and Smith (1998).

parallel direction is represented with black lines. The thick line shows the case of zero fault-parallel basal traction. We assume that these tractions are positive (Humphreys and Hager, 1990), and therefore the acceptable range of fault strengths must be below this line. Increasing fault-parallel basal tractions are shown with thin lines (Fig. 2).

Torque balance is represented with red lines, where the thick line represents zero fault-perpendicular basal tractions, and increasing tractions are shown with labeled thin red lines (Fig. 2). Counterclockwise rotation of the crust relative to the upper mantle (Humphreys and Hager, 1990) suggests that this motion applies clockwise torque to the block and therefore the allowable region is below the thick red line. Thus, Figure 2A relates fault strength and basal traction magnitudes. Given any two of these values the other two can be determined. For example, if the San

Andreas and San Jacinto fault strengths are each 30 MPa, the basal tractions necessary to satisfy force balance are ~ 14 MPa in the (NW) fault-parallel direction (black lines) and ~ 3.5 MPa at the northern end of the block in the (NE) fault-perpendicular direction (red lines).

The San Jacinto fault is younger, less organized (e.g., Wesnousky, 1988), and has less net offset than the San Andreas fault. Numerical modeling by Bird and Kong (1994) suggested that strike-slip fault strength is inversely related to net offset and the San Andreas fault is $\sim 30\%$ weaker than other Southern California strike-slip faults. Therefore we expect the San Jacinto fault to be as strong or stronger than the mature San Andreas fault. This limits the acceptable region to the stippled area of Figure 2A. The relative velocity of the mantle leading the upper crust toward the Transverse Ranges is at least twice any relative velocity due to rotation of the upper crust relative to the mantle (Humphreys and Hager, 1990). Therefore, for a given lower crustal viscosity, fault-parallel basal tractions should be at least two times larger than fault-perpendicular basal tractions, limiting the acceptable region to the right of the green line. A lower bound of fault-parallel basal tractions of ~ 3 MPa, based on the ~ 15 mm/yr of relative crust-mantle velocity in simple shear (Humphreys and Hager, 1990) and high-viscosity (1×10^{20} Pa-s) mafic lower crust (Fay and Humphreys, 2005), further limits the acceptable range of fault strengths and basal tractions to the shaded trapezoid (Fig. 2).

This shaded region represents our estimated range of possible fault strengths. The San Andreas fault is limited to ~ 21 – 35 MPa, and the San Jacinto fault to ~ 24 – 43 MPa (findings similar to those of Fialko et al., 2005). The maximum strength ratio of the San Jacinto and San Andreas faults is ~ 2 . This result suggests that younger or less active faults with less net offset, such as the San Jacinto and Elsinore faults, are not more than twice the strength of the mature San Andreas fault, consistent with results of Bird and Kong (1994).

The stress values we find represent averages over 30 km depth, although frictional faults typically extend to only ~ 15 km in Southern California. However, because a typical crustal strength profile is approximately triangular in shape (e.g., Brace and Kohlstedt, 1980; Scholz, 1988), the 30 km depth-averaged stress is nearly the same as the true upper crustal, 15 km depth-averaged fault strength. The maximum stress occurs at the brittle-ductile transition and is approximately twice the depth-averaged value. Thus, time-averaged stress at seismogenic mid-crustal depths is inferred to be ~ 42 – 86 MPa. Fur-

thermore, if fault strength in the ~ 15 -km-thick seismogenic upper crust is due to friction, the depth-averaged shear stress $\tau_{\bar{h}}$ is related to the effective friction coefficient f by $\tau_{\bar{h}} = fpgh/2$ (where ρ is density, g is gravitational acceleration, h is depth) (e.g., Savage and Lachenbruch, 2003), which gives a range of $f = 0.10$ – 0.21 , similar to 0.2 – 0.3 found by Townend and Zoback (2004). Fault-parallel basal traction acting to drive the NW motion and convergence of the Salton block into the Transverse Ranges is ~ 3 – 14 MPa, similar to the 8–14 MPa estimates of Bird and Kong (1994).

If the San Andreas and San Jacinto faults were significantly weaker than shown in Figure 2, the counterclockwise torque caused by the San Bernardino topography would cause an increase in fault-normal stress on the northern San Jacinto fault and a decrease on the San Andreas fault north of the Salton Sea. The opposite is generally observed; non-strike-slip strain from small earthquake focal mechanisms is a mixture of compression and extension along the San Jacinto fault (Sheridan, 1997), indicating that fault-normal deformation is not dominated by compression; fault-normal shortening in the Mecca–Indio Hills area of the San Andreas fault (Sheridan, 1997; Sylvester and Smith, 1976) indicates stresses normal to the San Andreas fault that produce counterclockwise torque on the Salton block. Thus, in this sense, the fault strength values we find are probably underestimated. However, the choice of the pole about which we sum torques (red dot in Fig. 1) emphasizes the torque caused by the mountains and our fault strength estimates. For example, if we calculate torque about the center of the block, the total range of acceptable depth-averaged fault strengths is ~ 13 – 33 MPa and the mean strength (the center of mass of the shaded region in Fig. 2A) is reduced for both faults by ~ 7 MPa. Given the kinematics of block rotation (Humphreys and Hager, 1990) and the approximately neutral San Andreas fault– and San Jacinto fault–perpendicular tectonics at the southern end of the block, the actual torque pole probably is in the southern third of the block, and the location (Fig. 1) we use is approximately correct.

DISCUSSION

Although we find San Andreas system faults to be relatively weak compared to lab experiments (Byerlee, 1978) and the surrounding crust (Townend and Zoback, 2000; Flesch et al., 2000), shear stresses of 21–43 MPa averaged over 30 km (42–86 MPa at mid-crustal depths) are larger than typical earthquake stress drops of 1–10 MPa, implying that, on average, these faults store $\geq \sim 4$ earthquakes

and do not necessarily rupture to zero shear stress.

This is consistent with time periods of relatively frequent and large events on the Mojave segment of the San Andreas fault (Weldon et al., 2004). A transient weakening mechanism (e.g., Brune et al., 1993; Di Toro et al., 2004) or self-healing effects during rupture (e.g., Fialko, 2004) may therefore be active during an earthquake, allowing rupture to end without exhausting all of the resolved shear stress.

Our modeling requires the forces and torques applied to the edges of the Salton block to sum to zero. This does not imply that stress within the block (e.g., on vertical planes parallel to the San Andreas fault) is constant or that the stress throughout is zero. On the contrary, stresses can vary with position and with time. For example, the increase or decrease in shear stress with distance from a strike-slip fault can be indicative of whether the fault is loaded by stresses applied from the side or from below (Lachenbruch and Sass, 1992). Furthermore, the fault strengths we find represent time-averaged tectonic stress on a fault, which on a shorter time scale increases gradually during the interseismic time and decreases rapidly during the earthquake. To maintain force and torque balance on a crustal block, the sudden coseismic stress drop must be balanced by some other load. The essentially instantaneous earthquake elastically stresses the surrounding lower crust and upper mantle, and these transient stresses, which provide some of the force to counteract the stress drop on the fault, decrease with time as the lower crust and upper mantle relax and tectonic loading on the fault increases (Perfettini and Avouac, 2004). The surface manifestation of this process is well documented in the postseismic transient signals seen in geodetic data (e.g., Thatcher, 1983; Freed and Bürgmann, 2004).

As in the southwestern United States (Atwater, 1970; Flesch et al., 2000), we find that Southern California deformation is driven by both plate interaction stresses transmitted laterally across faults and from below by basal tractions caused by flow driven by locally derived heterogeneous density structure. The fault tractions are found to be larger than basal tractions, although the total force from each mechanism suggests that either could be dominant. This relative importance is quantified in Figure 2B, where we contour the ratio of net driving force owing to fault and basal tractions. A value >1 indicates that basal tractions are relatively small and crustal deformation is driven largely by stresses transmitted laterally by block interaction. A ratio <1 indicates that fault driving and resisting forces nearly can-

cel, and mountain building at the leading edge of the block and basin formation at the trailing edge are driven by basal tractions. This would require a high-viscosity lower crust and similar San Andreas and San Jacinto fault strengths. The basal traction presumably caused by convergence and downwelling of mantle lithosphere beneath the Transverse Ranges (Bird and Rosenstock, 1984; Humphreys and Hager, 1990) is probably a special case of continental tectonics, and the general role of basal tractions in driving upper crustal block motion and deformation is debated (Jackson, 2002).

ACKNOWLEDGMENTS

This research was supported by the National Science Foundation (NSF) grant EAR-0106892 and the Southern California Earthquake Center (SCEC), funded by NSF cooperative agreement EAR-0106924 and U.S. Geological Survey Cooperative Agreement 02HQAG0008. This is SCEC contribution 867. Thorough reviews by Rick Bennett, Yuri Fialko, and an anonymous reviewer led to improvements in the content and presentation of this paper.

REFERENCES CITED

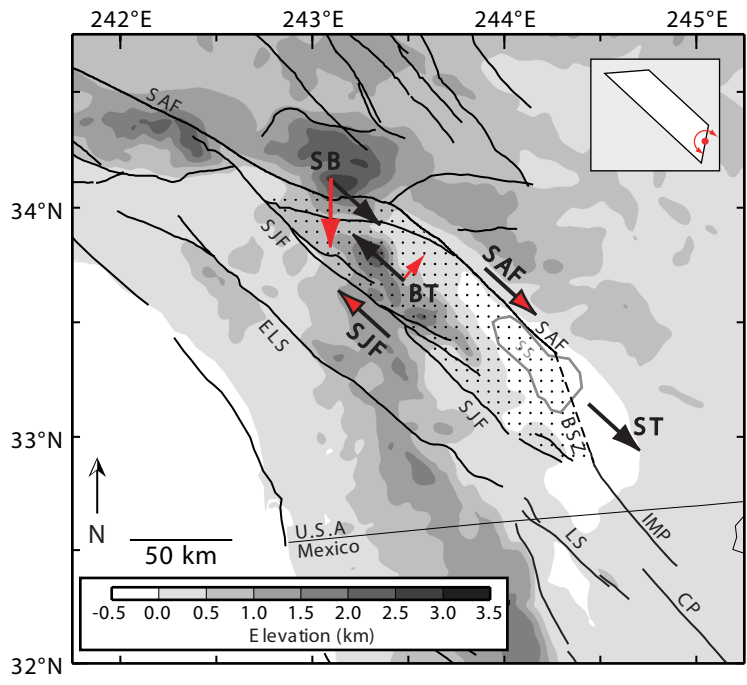
- Atwater, T., 1970, Implications of plate tectonics for the Cenozoic tectonic evolution of western North America: Geological Society of America Bulletin, v. 81, p. 3513–3536.
- Bennett, R.A., Friedrich, A.M., and Furlong, K.P., 2004, Codependent histories of the San Andreas and San Jacinto fault zones from inversion of fault displacement rates: *Geology*, v. 32, p. 961–964.
- Bird, P., and Kong, X., 1994, Computer simulations of California tectonics confirm very low strength of major faults: Geological Society of America Bulletin, v. 106, p. 159–174.
- Bird, P., and Rosenstock, R.W., 1984, Kinematics of present crust and mantle flow in Southern California: Geological Society of America Bulletin, v. 95, p. 946–957.
- Brace, W.F., and Kohlstedt, D.L., 1980, Limits on lithospheric stress imposed by laboratory measurements: *Journal of Geophysical Research*, v. 85, p. 6248–6252.
- Brune, J.N., Brown, S., and Johnson, P.A., 1993, Rupture mechanism and interface separation in foam rubber models of earthquakes; a possible solution to the heat flow paradox and the paradox of large overthrusts: *Tectonophysics*, v. 218, p. 59–67.
- Byerlee, J.D., 1978, Friction of rocks: *Pure and Applied Geophysics*, v. 116, p. 615–626.
- Di Toro, G., Goldsby, D.L., and Tullis, T.E., 2004, Friction falls towards zero in quartz rock as slip velocity approaches seismic rates: *Nature*, v. 427, p. 436–439.
- Fay, N.P., and Humphreys, E.D., 2005, Fault slip rates, effects of sediments and the strength of the lower crust in the Salton Trough region, Southern California: *Journal of Geophysical Research*, v. 110, p. B09401, doi: 10.1029/2004JB003548.
- Fialko, Y., 2004, Temperature fields generated by the elastodynamic propagation of shear cracks in the Earth: *Journal of Geophysical Research*, v. 109, p. B01303, doi: 10.1029/2003JB002497.
- Fialko, Y., Rivera, L., and Kanamori, H., 2005, Estimate of differential stress in the upper crust from variations in topography and strike along the San Andreas fault: *Geophysical Journal International*, v. 160, p. 527–532.
- Flesch, L.M., Holt, W.E., Haines, J.A., and Shentu, B., 2000, Dynamics of the Pacific–North American plate boundary in the western United States: *Science*, v. 287, p. 834–836.
- Freed, A., and Bürgmann, R., 2004, Evidence of power-law flow in the Mojave desert mantle: *Nature*, v. 430, p. 548–551.
- Fuis, G.S., Mooney, W.D., Healey, J.H., McMechan, G.A., and Lutter, W.J., 1982, Crustal structure of the Imperial Valley region: U.S. Geological Survey Professional Paper 1254, p. 25–49.
- Hardebeck, J.L., and Hauksson, E., 1999, Role of fluids in faulting inferred from stress field signatures: *Science*, v. 285, p. 236–239.
- Houseman, G.A., Neil, E.A., and Kohler, M.D., 2000, Lithospheric instability beneath the Transverse Ranges of California: *Journal of Geophysical Research*, v. 105, p. 16,237–16,250.
- Humphreys, E.D., and Hager, B.H., 1990, A kinematic model for the late Cenozoic development of Southern California crust and upper mantle: *Journal of Geophysical Research*, v. 95, p. 19,747–19,762.
- Jackson, J., 2002, Faulting, flow, and the strength of the continental lithosphere: *International Geology Review*, v. 44, p. 1–23.
- Jones, L.M., Hutton, L.K., Given, D.D., and Allen, C.R., 1986, The North Palm Springs, California, earthquake sequence of July 1986: *Seismological Society of America Bulletin*, v. 76, p. 1830–1837.
- Kanamori, H., and Anderson, D.L., 1975, Theoretical basis of some empirical relations in seismology: *Seismological Society of America Bulletin*, v. 65, p. 1073–1095.
- Kosloff, D., 1977, Numerical simulations of tectonic processes in Southern California: *Royal Astronomical Society Geophysical Journal*, v. 51, p. 487–501.
- Lachenbruch, A.H., and Sass, J.H., 1980, Heat flow and energetics of the San Andreas fault zone: *Journal of Geophysical Research*, v. 85, p. 6185–6222.
- Lachenbruch, A.H., and Sass, J.H., 1992, Heat flow from Cajon Pass, fault strength, and tectonic implications: *Journal of Geophysical Research*, v. 97, p. 4995–5015.
- Lachenbruch, A., Sass, J.H., and Galanis, S.P., 1985, Heat flow in southernmost California and the origin of the Salton Trough: *Journal of Geophysical Research*, v. 90, p. 6709–6736.
- Molnar, P., and Lyon-Caen, H., 1988, Some simple physical aspects of the support, structure, and evolution of mountain belts, in Clark, S.P., et al., eds., *Processes in continental lithospheric deformation*: Geological Society of America Special Paper 218, p. 179–207.
- Mount, V.S., and Suppe, J., 1987, State of stress near the San Andreas fault: Implications for wrench tectonics: *Geology*, v. 15, p. 1143–1146.
- Perfettini, H., and Avouac, H.-P., 2004, Stress transfer and strain rate variations during the seismic cycle: *Journal of Geophysical Research*, v. 109, p. B06402, doi: 10.1029/2003JB002917.
- Saffer, D.M., Bekins, B.A., and Hickman, S., 2003, Topographically driven groundwater flow and the San Andreas heat flow paradox revisited: *Journal of Geophysical Research*, v. 108, doi: 10.1029/2002JB001849.
- Savage, J.C., and Lachenbruch, A.H., 2003, Consequences of viscous drag beneath a transform fault: *Journal of Geophysical Research*, v. 108, 2025, doi:10.1029/2001JB000711.
- Scholz, C.H., 1988, The brittle-plastic transition and the depth of aseismic faulting: *Geologische Rundschau*, v. 77, p. 319–328.
- Scholz, C.H., 2000, Evidence for a strong San Andreas fault: *Geology*, v. 28, p. 163–166.
- Sheridan, J.M., 1997, Secondary deformation near strike-slip faults, Southern California [Ph.D. thesis]: Eugene, University of Oregon, 253 p.
- Sylvester, A.G., and Smith, R.B., 1976, Tectonic transpression and basement-deformation in San Andreas fault zone, Salton Trough, California: *American Association of Petroleum Geologists Bulletin*, v. 60, p. 2081–2102.
- Thatcher, W., 1983, Nonlinear strain buildup and the earthquake cycle on the San Andreas fault: *Journal of Geophysical Research*, v. 88, p. 5893–5902.
- Thatcher, W., Foulger, G.R., Julian, B.R., Svarc, J., Quilty, E., and Bawden, G.W., 1999, Present day deformation across the Basin and Range Province: *Science*, v. 282, p. 1714–1718.
- Townend, J., and Zoback, M.D., 2000, How faulting keeps the crust strong: *Geology*, v. 28, p. 399–402.
- Townend, J., and Zoback, M.D., 2001, Implications of earthquake focal mechanisms for the frictional strength of the San Andreas fault system, in Strachan, R.E., et al., eds., *The nature and tectonic significance of fault zone weakening*: Geological Society [London] Special Publication 186, p. 13–21.
- Townend, J., and Zoback, M.D., 2004, Regional tectonic stress near the San Andreas fault in central and Southern California: *Geophysical Research Letters*, v. 31, doi: 10.1029/2003GL018918.
- Weldon, R., Scharer, K., Fumal, T., and Biasi, G., 2004, Wrightwood and the earthquake cycle: What a long recurrence record tells us about how faults work: *GSA Today*, v. 14, p. 4–10.
- Wesnousky, S.G., 1988, Seismological and structural evolution of strike-slip faults: *Nature*, v. 335, p. 340–343.
- Wessel, P., and Smith, W.H.F., 1998, New, improved version of Generic Mapping Tools released: *Eos (Transactions, American Geophysical Union)*, v. 79, p. 579.
- Willett, S.D., and Brandon, M.T., 2002, On steady states in mountain belts: *Geology*, v. 30, p. 175–178.
- Zhu, L., and Kanamori, H., 2000, Moho depth variations in Southern California from teleseismic receiver functions: *Journal of Geophysical Research*, v. 105, p. 2969–2980.
- Zoback, M.D., Zoback, M.L., Mount, V.S., Suppe, J., Eaton, J.P., Healy, J.H., Oppenheimer, D.H., Reasenber, P.A., Jones, L.M., Raleigh, C.B., Wong, I.G., Scotti, O., and Wentworth, C.M., 1987, New evidence on the state of stress of the San Andreas fault system: *Science*, v. 238, p. 1105–1111.

Manuscript received 15 August 2005

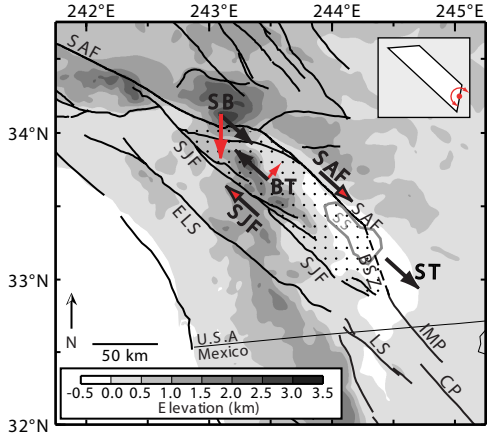
Revised manuscript received 23 November 2005

Manuscript accepted 7 December 2005

Printed in USA

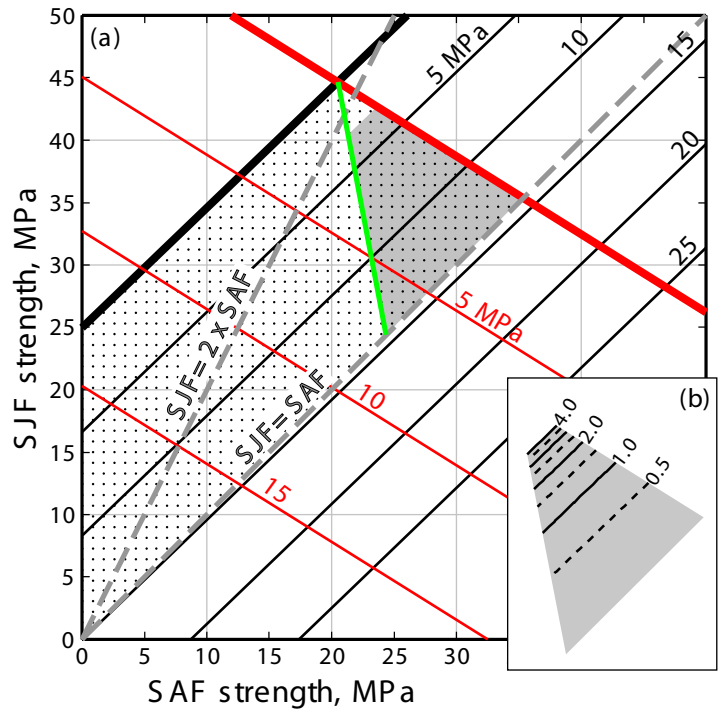


Original size

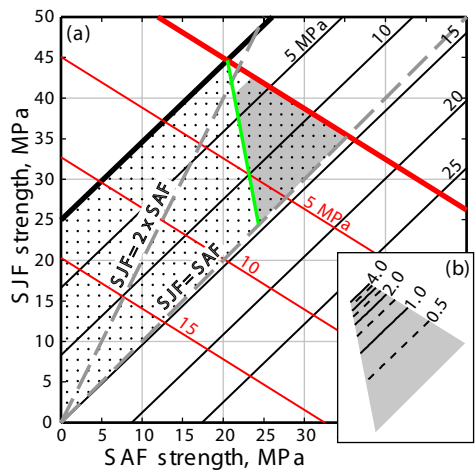


Reduced @ 64%

Figure 1, Fay and Humphreys, created with GMT and Illustrator v10, .eps



Original size



Reduced @ 65%

Figure 2, Fay and Humphreys, created with GMT and Illustrator v10, .eps